

Improvement in Muon Track Reconstruction with Robust Statistics

M. G. Aartsen², R. Abbasi²⁷, Y. Abdou²², M. Ackermann⁴¹, J. Adams¹⁵,
J. A. Aguilar²¹, M. Ahlers²⁷, D. Altmann⁹, J. Auffenberg²⁷, X. Bai^{31,1},
M. Baker²⁷, S. W. Barwick²³, V. Baum²⁸, R. Bay⁷, J. J. Beatty^{17,18},
S. Bechet¹², J. Becker Tjus¹⁰, K.-H. Becker⁴⁰, M. Bell³⁸,
M. L. Benabderrahmane⁴¹, S. BenZvi²⁷, J. Berdermann⁴¹, P. Berghaus⁴¹,
D. Berley¹⁶, E. Bernardini⁴¹, A. Bernhard³⁰, D. Bertrand¹², D. Z. Besson²⁵,
G. Binder^{8,7}, D. Bindig⁴⁰, M. Bissok¹, E. Blaufuss¹⁶, J. Blumenthal¹,
D. J. Boersma³⁹, S. Bohaichuk²⁰, C. Boehm³⁴, D. Bose¹³, S. Böser¹¹,
O. Botner³⁹, L. Brayeur¹³, H.-P. Bretz⁴¹, A. M. Brown¹⁵, R. Bruijn²⁴,
J. Brunner⁴¹, M. Carson²², J. Casey⁵, M. Casier¹³, D. Chirkin²⁷,
A. Christov²¹, B. Christy¹⁶, K. Clark³⁸, F. Clevermann¹⁹, S. Coenders¹,
S. Cohen²⁴, D. F. Cowen^{38,37}, A. H. Cruz Silva⁴¹, M. Danninger³⁴,
J. Daughhetee⁵, J. C. Davis¹⁷, C. De Clercq¹³, S. De Ridder²², P. Desiati²⁷,
M. de With⁹, T. DeYoung³⁸, J. C. Díaz-Vélez²⁷, M. Dunkman³⁸, R. Eagan³⁸,
B. Eberhardt²⁸, J. Eisch²⁷, R. W. Ellsworth¹⁶, S. Euler¹, P. A. Evenson³¹,
O. Fadiran²⁷, A. R. Fazely⁶, A. Fedynitch¹⁰, J. Feintzeig²⁷, T. Feusels²²,
K. Filimonov⁷, C. Finley³⁴, T. Fischer-Wasels⁴⁰, S. Flis³⁴, A. Franckowiak¹¹,
R. Franke⁴¹, K. Frantzen¹⁹, T. Fuchs¹⁹, T. K. Gaisser³¹, J. Gallagher²⁶,
L. Gerhardt^{8,7}, L. Gladstone²⁷, T. Glüsenkamp⁴¹, A. Goldschmidt⁸,
G. Golup¹³, J. A. Goodman¹⁶, D. Góra⁴¹, D. Grant²⁰, A. Groß³⁰,
M. Gurtner⁴⁰, C. Ha^{8,7}, A. Haj Ismail²², P. Hallen¹, A. Hallgren³⁹,
F. Halzen²⁷, K. Hanson¹², D. Heereman⁴², P. Heimann¹, D. Heinen¹,
K. Helbing⁴⁰, R. Hellauer¹⁶, S. Hickford¹⁵, G. C. Hill², K. D. Hoffman¹⁶,
R. Hoffmann⁴⁰, A. Homeier¹¹, K. Hoshina²⁷, W. Huelsnitz^{16,2}, P. O. Hulth³⁴,
K. Hultqvist³⁴, S. Hussain³¹, A. Ishihara¹⁴, E. Jacobi⁴¹, J. Jacobsen²⁷,
K. Jagielski¹, G. S. Japaridze⁴, K. Jero²⁷, O. Jlelati²², B. Kaminsky⁴¹,
A. Kappes⁹, T. Karg⁴¹, A. Karle²⁷, J. L. Kelley²⁷, J. Kiryluk³⁵, F. Kislak⁴¹,
J. Kläs⁴⁰, S. R. Klein^{8,7}, J.-H. Köhne¹⁹, G. Kohnen²⁹, H. Kolanoski⁹,
L. Köpke²⁸, C. Kopper²⁷, S. Kopper⁴⁰, D. J. Koskinen³⁸, M. Kowalski¹¹,
M. Krasberg²⁷, K. Krings¹, G. Kroll²⁸, J. Kunnen¹³, N. Kurahashi²⁷,
T. Kuwabara³¹, M. Labare¹³, H. Landsman²⁷, M. J. Larson³⁶,
M. Lesiak-Bzdak³⁵, M. Leuermann¹, J. Leute³⁰, J. Lünemann²⁸, J. Madsen³³,
R. Maruyama²⁷, K. Mase¹⁴, H. S. Matis⁸, F. McNally²⁷, K. Meagher¹⁶,
M. Merck²⁷, P. Mészáros^{37,38}, T. Meures¹², S. Miarecki^{8,7}, E. Middell⁴¹,

*Corresponding author. Email: wellons@icecube.wisc.edu, Phone: 304-542-4464, Address: Wisconsin Institutes for Discovery, 330 N. Orchard St., Madison, WI 53715

¹Physics Department, South Dakota School of Mines and Technology, Rapid City, SD 57701, USA

²Los Alamos National Laboratory, Los Alamos, NM 87545, USA

³also Sezione INFN, Dipartimento di Fisica, I-70126, Bari, Italy

⁴NASA Goddard Space Flight Center, Greenbelt, MD 20771, USA

37 N. Milke¹⁹, J. Miller¹³, L. Mohrmann⁴¹, T. Montaruli^{21,3}, R. Morse²⁷,
 38 R. Nahnhauser⁴¹, U. Naumann⁴⁰, H. Niederhausen³⁵, S. C. Nowicki²⁰,
 39 D. R. Nygren⁸, A. Obertacke⁴⁰, S. Odrowski³⁰, A. Olivas¹⁶, M. Olivo¹⁰,
 40 A. O’Murchadha¹², L. Paul¹, J. A. Pepper³⁶, C. Pérez de los Heros³⁹,
 41 C. Pfendner¹⁷, D. Pieloth¹⁹, N. Pirk⁴¹, J. Posselt⁴⁰, P. B. Price⁷,
 42 G. T. Przybylski⁸, L. Rädcl¹, K. Rawlins³, P. Redl¹⁶, R. Reimann¹,
 43 E. Resconi³⁰, W. Rhode¹⁹, M. Ribordy²⁴, M. Richman¹⁶, B. Riedel²⁷,
 44 J. P. Rodrigues²⁷, C. Rott¹⁷, T. Ruhe¹⁹, B. Ruzybayev³¹, D. Ryckbosch²²,
 45 S. M. Saba¹⁰, T. Salameh³⁸, H.-G. Sander²⁸, M. Santander²⁷, S. Sarkar³²,
 46 K. Schatto²⁸, M. Scheel¹, F. Scheriau¹⁹, T. Schmidt¹⁶, M. Schmitz¹⁹,
 47 S. Schoenen¹, S. Schöneberg¹⁰, L. Schönherr¹, A. Schönwald⁴¹, A. Schukraft¹,
 48 L. Schulte¹¹, O. Schulz³⁰, D. Seckel³¹, S. H. Seo³⁴, Y. Sestayo³⁰,
 49 S. Seunarine³³, C. Sheremata²⁰, M. W. E. Smith³⁸, M. Soiron¹, D. Soldin⁴⁰,
 50 G. M. Spiczak³³, C. Spiering⁴¹, M. Stamatikos^{17,4}, T. Stanev³¹, A. Stasik¹¹,
 51 T. Stezelberger⁸, R. G. Stokstad⁸, A. Stöbl⁴¹, E. A. Strahler¹³, R. Ström³⁹,
 52 G. W. Sullivan¹⁶, H. Taavola³⁹, I. Taboada⁵, A. Tamburro³¹,
 53 S. Ter-Antonyan⁶, S. Tilav³¹, P. A. Toale³⁶, S. Toscano²⁷, M. Usner¹¹,
 54 D. van der Drift^{8,7}, N. van Eijndhoven¹³, A. Van Overloop²², J. van Santen²⁷,
 55 M. Vehringer¹, M. Voge¹¹, M. Vraeghe²², C. Walck³⁴, T. Waldenmaier⁹,
 56 M. Wallraff¹, R. Wasserman³⁸, Ch. Weaver²⁷, M. Wellons^{27,*}, C. Wendt²⁷,
 57 S. Westerhoff²⁷, N. Whitehorn²⁷, K. Wiebe²⁸, C. H. Wiebusch¹,
 58 D. R. Williams³⁶, H. Wissing¹⁶, M. Wolf³⁴, T. R. Wood²⁰, K. Woschnagg⁷,
 59 C. Xu³¹, D. L. Xu³⁶, X. W. Xu⁶, J. P. Yanez⁴¹, G. Yodh²³, S. Yoshida¹⁴,
 60 P. Zarzhitsky³⁶, J. Ziemann¹⁹, S. Zierke¹, A. Zilles¹, M. Zoll³⁴, B. Recht⁴²,
 61 C. Ré⁴²

62 ¹III. Physikalisches Institut, RWTH Aachen University, D-52056 Aachen, Germany

63 ²School of Chemistry & Physics, University of Adelaide, Adelaide SA, 5005 Australia

64 ³Dept. of Physics and Astronomy, University of Alaska Anchorage, 3211 Providence Dr.,
 65 Anchorage, AK 99508, USA

66 ⁴CTSPS, Clark-Atlanta University, Atlanta, GA 30314, USA

67 ⁵School of Physics and Center for Relativistic Astrophysics, Georgia Institute of
 68 Technology, Atlanta, GA 30332, USA

69 ⁶Dept. of Physics, Southern University, Baton Rouge, LA 70813, USA

70 ⁷Dept. of Physics, University of California, Berkeley, CA 94720, USA

71 ⁸Lawrence Berkeley National Laboratory, Berkeley, CA 94720, USA

72 ⁹Institut für Physik, Humboldt-Universität zu Berlin, D-12489 Berlin, Germany

73 ¹⁰Fakultät für Physik & Astronomie, Ruhr-Universität Bochum, D-44780 Bochum,
 74 Germany

75 ¹¹Physikalisches Institut, Universität Bonn, Nussallee 12, D-53115 Bonn, Germany

76 ¹²Université Libre de Bruxelles, Science Faculty CP230, B-1050 Brussels, Belgium

77 ¹³Vrije Universiteit Brussel, Dienst ELEM, B-1050 Brussels, Belgium

78 ¹⁴Dept. of Physics, Chiba University, Chiba 263-8522, Japan

79 ¹⁵Dept. of Physics and Astronomy, University of Canterbury, Private Bag 4800,
 80 Christchurch, New Zealand

81 ¹⁶Dept. of Physics, University of Maryland, College Park, MD 20742, USA

82 ¹⁷Dept. of Physics and Center for Cosmology and Astro-Particle Physics, Ohio State
 83 University, Columbus, OH 43210, USA

84 ¹⁸Dept. of Astronomy, Ohio State University, Columbus, OH 43210, USA

85 ¹⁹Dept. of Physics, TU Dortmund University, D-44221 Dortmund, Germany

86 ²⁰Dept. of Physics, University of Alberta, Edmonton, Alberta, Canada T6G 2E1

- 87 ²¹*Département de physique nucléaire et corpusculaire, Université de Genève, CH-1211*
88 *Genève, Switzerland*
- 89 ²²*Dept. of Physics and Astronomy, University of Gent, B-9000 Gent, Belgium*
- 90 ²³*Dept. of Physics and Astronomy, University of California, Irvine, CA 92697, USA*
- 91 ²⁴*Laboratory for High Energy Physics, École Polytechnique Fédérale, CH-1015 Lausanne,*
92 *Switzerland*
- 93 ²⁵*Dept. of Physics and Astronomy, University of Kansas, Lawrence, KS 66045, USA*
- 94 ²⁶*Dept. of Astronomy, University of Wisconsin, Madison, WI 53706, USA*
- 95 ²⁷*Dept. of Physics and Wisconsin IceCube Particle Astrophysics Center, University of*
96 *Wisconsin, Madison, WI 53706, USA*
- 97 ²⁸*Institute of Physics, University of Mainz, Staudinger Weg 7, D-55099 Mainz, Germany*
- 98 ²⁹*Université de Mons, 7000 Mons, Belgium*
- 99 ³⁰*T.U. Munich, D-85748 Garching, Germany*
- 100 ³¹*Bartol Research Institute and Department of Physics and Astronomy, University of*
101 *Delaware, Newark, DE 19716, USA*
- 102 ³²*Dept. of Physics, University of Oxford, 1 Keble Road, Oxford OX1 3NP, UK*
- 103 ³³*Dept. of Physics, University of Wisconsin, River Falls, WI 54022, USA*
- 104 ³⁴*Oskar Klein Centre and Dept. of Physics, Stockholm University, SE-10691 Stockholm,*
105 *Sweden*
- 106 ³⁵*Department of Physics and Astronomy, Stony Brook University, Stony Brook, NY*
107 *11794-3800, USA*
- 108 ³⁶*Dept. of Physics and Astronomy, University of Alabama, Tuscaloosa, AL 35487, USA*
- 109 ³⁷*Dept. of Astronomy and Astrophysics, Pennsylvania State University, University Park,*
110 *PA 16802, USA*
- 111 ³⁸*Dept. of Physics, Pennsylvania State University, University Park, PA 16802, USA*
- 112 ³⁹*Dept. of Physics and Astronomy, Uppsala University, Box 516, S-75120 Uppsala, Sweden*
- 113 ⁴⁰*Dept. of Physics, University of Wuppertal, D-42119 Wuppertal, Germany*
- 114 ⁴¹*DESY, D-15735 Zeuthen, Germany*
- 115 ⁴²*Dept. of Computer Sciences, University of Wisconsin, Madison, WI 53706, USA*

116 **Abstract**

117 The IceCube detector is a high-energy neutrino telescope located at the geo-
118 graphic South Pole. Neutrinos cannot be directly observed and must be inferred
119 from their interactions with other particles. These interactions sometimes gener-
120 ate a muon, which in turn emits observable light. At the energies the IceCube
121 detector is sensitive to, the neutrino and generated muon have almost parallel
122 paths, so the neutrino path can be inferred from a reconstruction of the muon
123 path. However, reconstructing the muon path from the observed light is chal-
124 lenging due to noise, outliers in the data, and the possibility of simultaneously
125 multiple muons inside the detector.

126 This manuscript describes our work on two problems: (1) the *path recon-*
127 *struction* problem, in which, given a set of observations, our goal is to recover
128 the path of a muon, and (2) the *coincident event* problem, which is to deter-
129 mine how many muons are active in the detector during a time window. Rather
130 than solving these problems by developing more complex physical models, our
131 approach is to augment the detector's current models with simple filters and
132 robust statistical techniques. Using the metric of median angular resolution,
133 a standard metric for path reconstruction, our solution improves the accuracy

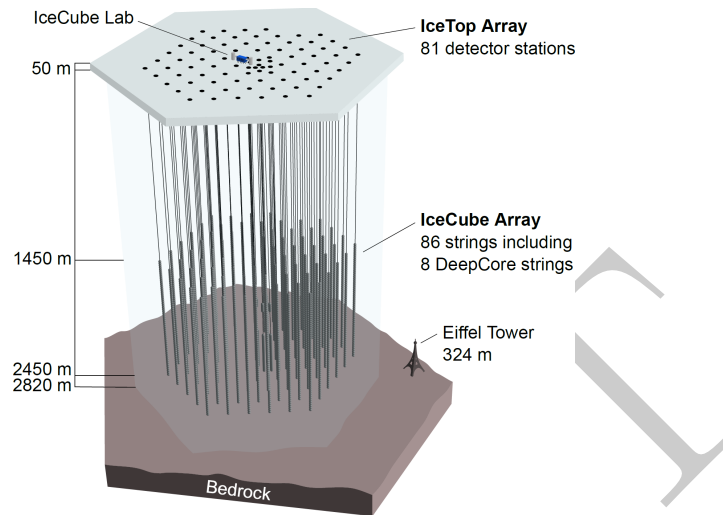


Figure 1: The IceCube neutrino detector in the Antarctic ice. A picture of the Eiffel Tower is shown for scale.

134 in the reconstruction direction by 13%. Our solution for the coincident-event
 135 problem accurately determines the number of muons 98% of the time, which is
 136 an improvement of 86% over the software previously used in IceCube.

137 *Keywords:* IceCube, Track reconstruction, Neutrino telescope, Neutrino
 138 astrophysics, Robust Statistics

139 **1. Introduction**

140 The IceCube neutrino detector searches for neutrinos that are generated by
 141 the universe’s most violent astrophysical events: exploding stars, gamma ray
 142 bursts, and cataclysmic phenomena involving black holes and neutron stars [1].
 143 The detector, roughly a cubic kilometer in size, is located near the geographic
 144 South Pole and is buried to a depth of about 2.5 km in the Antarctic ice [2].
 145 The detector is illustrated in Figure 1 and a more complete description is given
 146 in Section 2.

147 We examine two problems that arise in the IceCube detector’s neutrino
 148 detection:

- 149 1. *Reconstruction*, in which the path of a muon is reconstructed from the
 150 observed light at different positions and times in the detector.
- 151 2. *Coincident Event Detection*, in which we detect the number of muons
 152 inside the detector, and assign observed photons to a muon.

153 The IceCube Collaboration has spent considerable effort on both of these
154 problems over the last decade, as they are a critical step for data analysis.
155 They have developed sophisticated domain models that take into account the
156 interaction of near- and far-field effects of light, and have undertaken complex
157 mapping efforts to understand the effects of photon propagation in the ice [3,
158 4]. Our solutions do not further refine the detailed modeling of these physical
159 effects, but instead augment the models with off-the-shelf statistical techniques
160 combined with some simple data filtering to remove outliers.

161 *Related Work.* Track reconstruction and coincident event detection challenges
162 are ubiquitous in particle physics [5–7], both in particle accelerators and cosmic
163 particle detectors. While the work described in this manuscript builds on the
164 previous technique developed for the IceCube detector [3], our techniques are
165 general purpose, and potentially have applications in detectors beyond IceCube.

166 *Outline.* We begin by describing the necessary background on the IceCube de-
167 tector in Section 2. In Section 3, we describe the reconstruction pipeline in-
168 cluding the prior IceCube software, then we discuss our work and its results.
169 Section 4 describes our work on coincident event detection, and follows a parallel
170 structure to Section 3. We describe how in this application, a simple heuristic
171 approach is an improvement over the prior software. We close with a conclusion
172 in Section 5.

173 2. Background

174 The IceCube detector is composed of 5160 optical detectors, each composed
175 of a photomultiplier tube (PMT) and onboard digitizer[8]. The PMTs are spread
176 over 86 vertical strings arranged in a hexagonal shape, with a total instrumented
177 volume of approximately a cubic kilometer. The PMTs on a given string are sep-
178 arated vertically by 17 m, and the string-to-string separation is roughly 125 m.

179 When a neutrino enters the telescope, it sometimes interacts with the ice
180 and generates a muon. As the muon travels through the detector, it radiates
181 light[9], which is observed by the PMTs and broken down into discrete *hits*[10].
182 A collection of hits is called an *event*, and if the number of hits in an event is
183 sufficiently large, the muon path reconstruction algorithm is triggered.

184 2.1. Cosmic Ray Background

185 In addition to neutrinos, muons can also be generated by cosmic rays. Ice-
186 Cube analyses on neutrinos are not interested in cosmic ray muons, and the de-
187 tector attempts to separate out the cosmic ray muons from the neutrino muons.

188 The primary mechanism for this separation is reconstructing the muon path,
189 and determining if the muon was traveling downwards into the Earth or upwards
190 out of the Earth. Since neutrinos can penetrate the Earth but cosmic ray muons
191 cannot, it follows that a muon traveling out of the Earth must have been caused
192 by a neutrino. Thus, by selecting only the muons that are reconstructed as
193 up-going, the cosmic ray muons can, in principle, be removed from the data.

194 2.2. Challenges in Neutrino Detection

195 Recovering the muon path from the light measurements is the *reconstruction*
196 *problem*. The reconstruction algorithms used in the detector have several
197 challenges, which must be overcome. The underlying mechanics are stochastic
198 and incompletely modeled, the data is noisy and contains outliers, and the
199 computational abilities of the detector are limited.

200 *Modeling Difficulties.* The underlying physics of the system are nontrivial to
201 model. The muon's light is scattered by the dust and air crystals in the ice
202 medium. This scattering is both complex and stochastic, and the scattering
203 properties of the ice vary with depth [11].

204 *Noise.* An unescapable challenge is the noise inherent in the data. The PMTs
205 are so sensitive to light that they can record hits even in the absence of nearby
206 muons. These hits can arise from photons generated either by radioactive decay
207 inside the PMT or the triboluminescence [12] of the ice.

208 *Computational Constraints.* The reconstruction algorithms are also limited in
209 complexity by the computing resources available at the South Pole. The path
210 reconstruction algorithm has to process about 3000 muons per second, so algo-
211 rithms with excessive computational demands are discouraged.

212 *Cosmic Ray to Neutrino Ratio.* While the cosmic ray muons can in principle
213 be removed by selecting only muons reconstructed as up-going, the number of
214 observed cosmic ray muons exceeds the number of observed neutrino muons by
215 five orders of magnitude [3]. Thus, high accuracy reconstructions are critical
216 for preventing erroneously reconstructed cosmic ray muons from dominating the
217 neutrino analysis.

218 3. Reconstruction Problem

219 By augmenting the reconstruction algorithm with some simple filters and
220 classical data analysis techniques, we show significant improvement in the re-
221 construction algorithm's accuracy.

222 3.1. Prior IceCube Software

223 The muon path reconstruction process (outlined in Figure 2) starts when
224 the number of detected hits exceeds a preset threshold and the data collection
225 step triggers. After the initial data is collected, it then passes through a series
226 of simple filters to remove obvious outliers, described more in [13].

227 This is followed by a simple reconstruction algorithm *linefit*, which simply
228 finds the track that minimizes the sum of the squares of the distances between
229 the track and the hits. More formally, assume there are N hits, and denote the
230 position and time of the i th hit as \vec{x}_i and t_i respectively. Let the reconstructed
231 muon path have a velocity of \vec{v} , and let the reconstructed path pass through point

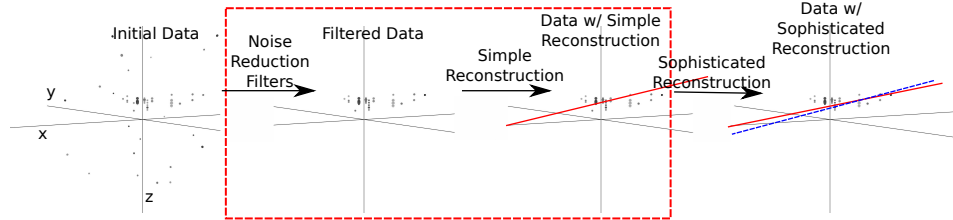


Figure 2: The reconstruction pipeline used to process data in the IceCube detector. After initial data is collected, it is then processed by some simple noise filters, which remove clear outliers. This cleaned data is processed by a simple reconstruction algorithm (red line), which is used as the seed for the more sophisticated reconstruction algorithm (dashed blue line). The sophisticated reconstruction is then evaluated as a potential neutrino. Our work in the reconstruction problem makes changes to the filtering and simple reconstruction step (indicated by the dashed red box).

232 \vec{x}_0 at time t_0 . Then linefit reconstruction solves the *least-squares* optimization
 233 problem

$$\min_{t_0, \vec{x}_0, \vec{v}} \sum_{i=1}^N \rho_i(t_0, \vec{x}_0, \vec{v})^2, \quad (1)$$

234 where

$$\rho_i(t_0, \vec{x}_0, \vec{v}) = \|\vec{v}(t_i - t_0) + \vec{x}_0 - \vec{x}_i\|_2. \quad (2)$$

235 The linefit reconstruction is primarily used to generate an initial track or *seed*
 236 for a more sophisticated reconstruction.

237 The reconstruction algorithm used in the sophisticated reconstruction *SPE*,
 238 is described further in [3]. *SPE* takes as input the least-squares reconstruction
 239 and the event data, and uses a likelihood maximization algorithm to reconstruct
 240 the muon path.

241 3.2. Algorithm Improvement

242 *SPE* is dependent on the seed. Given a seed that is inaccurate by greater than
 243 or equal to 6° , *SPE* typically cannot recover, and also produces a reconstruction
 244 inaccurate by greater than or equal to 6° . In addition, the likelihood space for
 245 *SPE* can contain multiple local maxima, so improving the accuracy of a seed
 246 already near the true solution still improves the accuracy of *SPE*. Thus, we
 247 focused our work on improving the quality of the seed.

248 As indicated in Equation 1, a least-squares fit models the muon as a single
 249 point moving in a straight line, and hits are penalized quadratically in their
 250 distance from this line. Thus there is an implicit assumption in this model,
 251 which is that all the hits will be near the muon. There are several pitfalls in
 252 this assumption:

- 253 1. It ignores the scattering effects of the ice medium. Some of the photons can
 254 scatter for over a microsecond, which means that when they are recorded
 255 by a PMT, the muon will be over 300 m away.

256 2. While the noise reduction steps remove most of the outlier noise, the noise
 257 hits that survive can be far from the muon. Since these outliers are given
 258 quadratic weight, they exert a huge influence over the model.

259 The first pitfall is a case of the model being incomplete and not modeling
 260 the data, and the second amounts to the model not being robust to noise. Our
 261 solution was twofold: improve the model and increase the noise robustness by
 262 replacing least squares with robust statistical techniques.

263 3.2.1. Improving the Model

264 The least-squares model does not model the scattering, and thus hits gen-
 265 erated by photons that scattered for a significant length of time are not useful
 266 predictors of the muon’s position. We found that a simple filter could identify
 267 these scattered hits, and generate an accuracy improvement of almost a factor
 268 of two by removing them from the dataset.

269 More formally, for each hit h_i , the algorithm looks at all neighboring hits
 270 within a neighborhood of r , and if there exists a neighboring hit h_j with a time
 271 stamp that is t earlier than h_i , then h_i is considered a scattered hit, and is not
 272 used in the simple reconstruction algorithm. Optimal values of r and t were
 273 found to be 156 m and 778 ns by parameter search.

274 3.2.2. Adding Robustness to Noise

275 One of the fundamental problems with least squares is that outliers are given
 276 a quadratic influence, whereas an ideal model would give outliers zero influence.
 277 Such an ideal model does not exist, but classical statistics has developed models
 278 where outliers can be marginalized. We experimented replacing the least-squares
 279 model with a variety of more robust models: a deadzone-linear fit, a one-norm
 280 fit, and a Huber fit [14].

281 Of the models that we tested, the Huber penalty function gave the greatest
 282 increase in reconstruction accuracy. More formally, we replace Equation 1 with
 283 the optimization problem

$$\min_{t_0, \vec{x}_0, \vec{v}} \sum_{i=1}^N \phi(\rho_i(t_0, \vec{x}_0, \vec{v})), \quad (3)$$

284 where the Huber penalty function $\phi(\rho)$ is defined as

$$\phi(\rho) \equiv \begin{cases} \rho^2 & \text{if } \rho < \mu \\ \mu(2\rho - \mu) & \text{if } \rho \geq \mu \end{cases}. \quad (4)$$

285 Here, $\rho_i(t_0, \vec{x}, \vec{v})$ is defined in Equation 2 and μ is a constant calibrated to the
 286 data (in our work, the optimal value of μ is 153 m).

287 The Huber penalty function has two regimes. In the near-hit regime ($\rho < \mu$)
 288 hits are assumed to be strongly correlated with the muon’s path, and the Huber
 289 penalty function behaves like least squares, giving these hits quadratic weight.
 290 In the far-hit regime ($\rho \geq \mu$), hits are given linear weights as they are more
 291 likely to be noise.

Table 1: Median angular resolution (degrees) for reconstruction improvements. The first line is the accuracy of the prior least-squares model, and the subsequent lines are the accuracy measurements from cumulatively adding improvements into the simple reconstruction algorithm.

Algorithm	θ_{med}
Linefit Reconstruction (Least-Squares)	9.917
With Addition of Logical Filter	5.205
With Addition of Huber Regression	4.672
With Addition of Outlier Removal	4.211

292 In addition to its attractive robustness properties, the Huber fit’s weight
 293 assignment also has the added benefit that it inherently labels points as outliers
 294 (those with $\rho \geq \mu$). Thus, once the Huber fit is computed, we can go one step
 295 farther and simply remove the labeled outliers from the dataset. A better fit is
 296 then obtained by computing the least-squares fit on the data with the outliers
 297 removed.

298 3.3. Results

299 To measure the improvement generated by our changes, we use the metric of
 300 *median angular resolution* θ_{med} , which is a standard metric used in the collab-
 301 oration. The angular resolution of a reconstruction is the arc-distance between
 302 the reconstruction and the true path. Removing the scattered hits and adding
 303 robustness to the model generates measurable a improvement to the model’s
 304 accuracy, as shown in Table 1.

305 We can improve the median angular resolution of the simple reconstruction
 306 by 57.6%. Seeding SPE with the improved simple reconstruction generates an
 307 improvement in the angular resolution of 12.9%. These improvements in the
 308 reconstruction algorithm result in 10% fewer atmospheric muons erroneously
 309 reconstructed as up-going, and 1% more muons correctly reconstructed as up-
 310 going.

311 4. Coincident Event Problem

312 In our second experiment, we look at the problem of determining when more
 313 than one muon has entered the detector. In the most common case, a single
 314 muon will pass though the detector and generate an event before exiting. These
 315 events are processed by the pipeline described in Figure 2. However, for roughly
 316 9% of the events collected by the data collection algorithm, more than one muon
 317 will be passing though the detector simultaneously, an occurrence known as a
 318 *coincident event*.

319 One of the primary sources of background noise in the scientific analyses
 320 of the IceCube Collaboration is coincident background muons that have been
 321 erroneously reconstructed as neutrinos. To see why this occurs, consider the
 322 coincident event shown in Figure 3. There are two clear groups of hits; how-
 323 ever, the reconstruction algorithm treats them as a single group, resulting in a

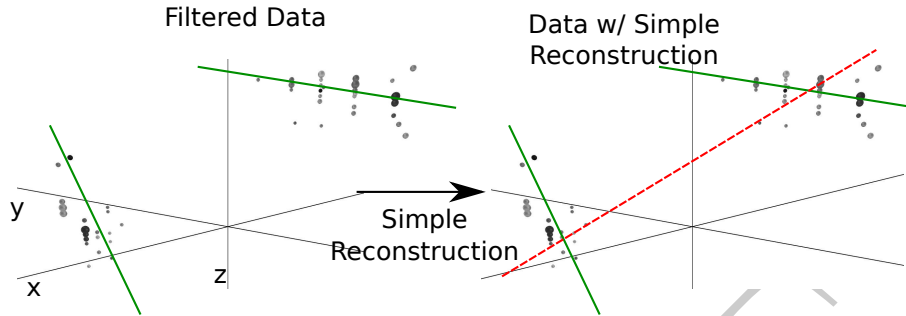


Figure 3: In this example, an event that is clearly composed of two muons (actual tracks shown as green thick lines) is treated as a single muon, and thus the reconstruction (shown in dashed red) is inaccurate.

erroneous reconstruction. In the ideal case, the reconstruction algorithm would identify coincident events and split them, as in Figure 4.

The challenge in this example is determining the number of muons in an event. In our results, we find that a simple spatial clustering algorithm can solve this classification problem with less than 2% error.

4.1. Prior IceCube Software

Coincident events have been a concern in the IceCube analysis [15] for years, and some software has been developed to handle coincident events. As a baseline of comparison, we use the *TTrigger* software, which is described in [16].

4.2. Algorithm Improvement

Our solution to this problem is a proximal clustering algorithm. The intuition in proximal clustering is that points local in space and time are probably from the same muon. The proximal clustering algorithm iterates through each pair of hits (i, j) and builds an adjacency matrix \mathbf{A} as

$$\mathbf{A}_{ij} = \begin{cases} 1 & \text{if } \|\Delta x^2 + \Delta y^2 + \Delta z^2 + (c\Delta t)^2\|_2 \leq \alpha, \\ 0 & \text{otherwise} \end{cases} \quad (5)$$

where $\Delta x, \Delta y, \Delta z$ and Δt are the space and time differences between the pair of hits, and α is tuned to the data. The clustering can be recovered by extracting the connected components of the graph defined by \mathbf{A} .

4.2.1. Improving the Model

When implemented naively, proximal clustering succeeded for the majority of the events, but failed if there was a gap in the muon track, which can occur when the muon travels through dusty ice. If there is a significantly large gap, the algorithm erroneously separates the hits into two clusters.

To get around this, an additional heuristic is added, *track connecting*. After the data segmentation is finished, track connecting determines if separate

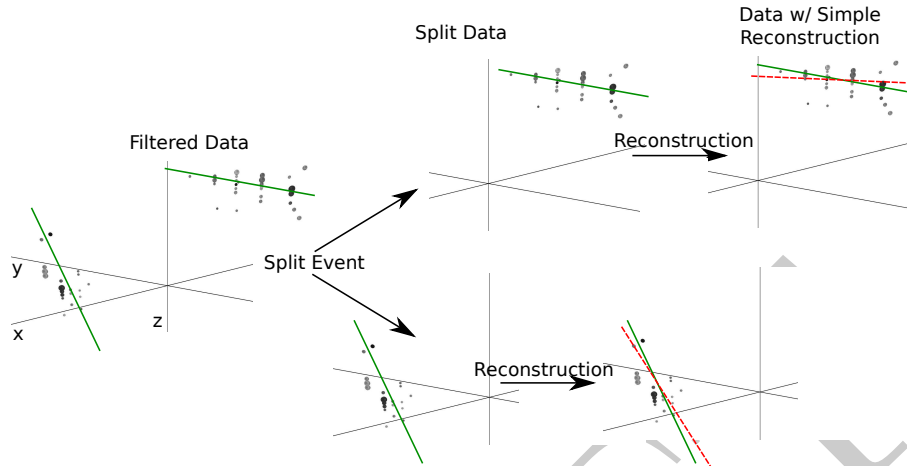


Figure 4: Ideally, the detector would split coincident events before computing the reconstruction. Splitting the event results in more accurate reconstructions (reconstructions shown in red, true muon tracks shown in green). Note the difference in the reconstructions compared with Figure 3.

348 clusters should be combined. It computes the mean position and time of each
 349 cluster, and connects a hypothetical muon track t between each pair of sub-
 350 spaces.

351 It checks if the speed s of the hypothetical path is within 25% of the speed of
 352 light c , and it checks that the mean distance between hits and t in both clusters
 353 is less than 60 m. If t passes both checks, the clusters are combined.

354 4.2.2. Adding Robustness to Noise

355 Proximal clustering is susceptible to noise. Noise hits close to two disjoint
 356 tracks will be considered adjacent to both tracks, connecting the two tracks in
 357 the adjacency matrix.

358 One heuristic that worked well at mitigating this problem was to use all the
 359 hits in building the adjacency matrix. During data collection, some hits are
 360 marked as coincident, which indicates that both they and a neighboring PMT
 361 reported a hit. These hits have a high probability of not being noise hits, and
 362 thus exclusively using them to build the adjacency matrix mitigates the problem
 363 of erroneously connecting two tracks.

364 After the proximal clustering algorithm has extracted the tracks from the
 365 adjacency matrix, the hits not used in the construction of the adjacency matrix
 366 are simply assigned to the closest reconstructed track.

367 4.3. Results

368 There were two competing goals for coincident event detection algorithms:
 369 the algorithm should be conservative enough that events containing single paths

Table 2: Error Rates for Classification Algorithms

Algorithm	$E_{\text{Single}} \%$	$E_{\text{Multiple}} \%$	$E_{\text{tot}} \%$
Trivial	0.0	100.0	8.3
TTrigger	11.5	31.8	13.2
Proximal clustering	0.2	18.9	1.8

370 are not erroneously split, and aggressive enough that a useful fraction of coin-
 371 cident events are split correctly. Erroneously discarding events containing neu-
 372 trinos is worse than erroneously allowing additional noise into the data pool,
 373 as noise can be eliminated by future filtering of the data pool. Our algorithm
 374 is tuned to keep almost all of the single events correctly unsplit, while still
 375 correctly splitting 80% of the coincident events.

376 4.3.1. Measurements

377 We modified the reconstruction pipeline shown in Figure 2, in between the
 378 noise cleaning and the simple reconstruction, by adding a step for coincident
 379 event detection, as shown in Figure 4. This step takes cleaned data and attempts
 380 to classify the event as a single-track or multiple-track event.

381 We ran each algorithm on two datasets of simulated data. One dataset
 382 comprised single-muon events, and the other dataset comprised multiple-muon
 383 events. In each dataset, we measured the classification error E , which is the
 384 fraction of events that were misclassified. To get a global measurement, we
 385 compute the *total error* E_{tot} , defined as

$$E_{\text{tot}} = w_{\text{Single}} E_{\text{Single}} + w_{\text{Multiple}} E_{\text{Multiple}}. \quad (6)$$

386 For computing E_{tot} , we use $w_{\text{Single}} = 0.917$ and $w_{\text{Multiple}} = 0.083$, which is
 387 the frequency in which single-muon and multiple-muon events appear in data
 388 simulating the distribution of events that trigger the reconstruction algorithm.

389 We present our results for the coincident event problem by measuring how
 390 well each algorithm performs at determining the number of subspaces in an
 391 event.

392 There are two natural comparisons for our work: the prior software TTrigger,
 393 as well as the trivial algorithm, which always classifies each event as a single-
 394 track event. Clearly, the latter will always get the single-track events correct,
 395 and always get the multiple-track events wrong. We provide a comparison of
 396 these techniques in Table 2. As shown, our software classifies the number of
 397 muons in the detector 86% better than TTrigger.

398 5. Conclusions

399 The challenges in the IceCube detector are complex. Despite this complexity,
 400 we found that we can achieve significant improvement via classical data analysis
 401 algorithms and simple models.

402 We looked at the problem of general reconstruction improvement, and found
403 that by applying a simple filter to the data and adding some robustness to the
404 fitting algorithm, we got superior reconstructions in the noisy environments of
405 the IceCube data. Our reconstruction software runs on-site, and is included in
406 all IceCube analysis.

407 We also looked at the problem of determining the number of muons in the
408 detector. We found that proximal clustering, the simplest algorithm that we
409 tried, was as good as or better than all other tested algorithms. Our proximal
410 clustering algorithm was an 86% improvement over the current software.

411 References

- 412 [1] IceCube Collaboration, IceCube webpage, <http://icecube.wisc.edu/>.
- 413 [2] IceCube Collaboration, First year performance of the IceCube neutrino
414 telescope, *Astroparticle Physics* 26 (3) (2006) 155–173.
- 415 [3] IceCube Collaboration, Muon Track Reconstruction and Data Selection
416 Techniques in AMANDA, *Nuclear Instruments and Methods in Physics
417 Research Section A* 524 (2004) 169–194.
- 418 [4] IceCube Collaboration, Measurement of South Pole ice transparency with
419 the IceCube LED calibration system IceCube Collaboration, *Nuclear In-
420 struments and Methods in Physics Research Section A*.
- 421 [5] ATLAS Collaboration, Tracking and vertexing with the ATLAS detector at
422 the LHC, *Nuclear Instruments and Methods in Physics Research Section A:
423 Accelerators, Spectrometers, Detectors and Associated Equipment* 650 (1)
424 (2011) 218–223.
- 425 [6] R. S. Chivukulaa, M. Goldena, E. H. Simmons, Multi-jet physics at hadron
426 colliders, *Nuclear Physics B* 363 (1) (1991) 83–96.
- 427 [7] S. Ellis, J. Huston, K. Hatakeyama, P. Loch, M. Tönnesmann, Jets in
428 hadron–hadron collisions, *Progress in Particle and Nuclear Physics* (60)
429 (2008) 484–551.
- 430 [8] IceCube Collaboration, Calibration and characterization of the IceCube
431 photomultiplier tube, *Nuclear Instruments and Methods in Physics Re-
432 search Section A* 618 (2010) 139–152.
- 433 [9] IceCube Collaboration, An improved method for measuring muon energy
434 using the truncated mean of dE/dx , *Nuclear Instruments and Methods in
435 Physics Research Section A*.
- 436 [10] IceCube Collaboration, The icecube data acquisition system: Signal cap-
437 ture, digitization, and timestamping, *Nuclear Instruments and Methods in
438 Physics Research Section A* 601 (3) (2009) 294–316.

- 439 [11] M. Wolf, E. Resconi, Verification of South Pole glacial ice simulations in Ice-
440 Cube and its relation to conventional and new, accelerated photon tracking
441 techniques, Master's thesis, Max-Planck-Institut für Kernphysik Heidelberg
442 (September 2010).
- 443 [12] IceCube Collaboration, IceCube sensitivity for low-energy neutrinos from
444 nearby supernovae, *Astronomy & Astrophysics* 535 (A109) (2011) 18.
- 445 [13] M. Ackermann, Searches for signals from cosmic point-like sources of high
446 energy neutrinos in 5 years of AMANDA-II data, Ph.D. thesis, Humboldt-
447 Universität zu Berlin (2006).
- 448 [14] S. Boyd, L. Vandenberghe, *Convex Optimization*, Cambridge University
449 Press, 2009.
- 450 [15] IceCube Collaboration, Measurement of the atmospheric neutrino energy
451 spectrum from 100 GeV to 400 TeV with IceCube, *Physical Review D*
452 83 (1).
- 453 [16] D. Chirkin, Measurement of the atmospheric neutrino energy spectrum
454 with IceCube, Proceedings of the 31st ICRC.